Proceedings of the ASME 2017 International Mechanical Engineering Congress and Exposition
IMECE2017
November 3-9, 2017, Tampa, Florida, USA

IMECE2017-72162

THERMAL DISCOMFORT DETECTION USING THERMAL IMAGING

Mihai Burzo*
Mechanical Engineering
University of Michigan-Flint
Flint, MI 48502, USA
mburzo@umich.edu

Mohamed Abouelenien
Computer Science and Engineering
University of Michigan
Ann Arbor, MI 48109, USA
zmohamed@umich.edu

David Van Alstine
Mechanical Engineering
University of Michigan, Flint
Flint, MI 48502, USA
davidjv@umflint.edu

Kristen Rusinek
Mechanical Engineering
University of Michigan, Flint
Flint, MI 48502, USA
krusinek@umflint.edu

ABSTRACT

Effective energy management in the buildings is one of the key factors impacting the overall energy consumption, and thus has important consequences on climate and the environment. Detecting human thermal discomfort can be potentially used to reduce energy consumption in both buildings and vehicles, while maintaining the thermal comfort sensation of the occupants. This paper proposes a non-contact approach that relies on the thermal features obtained from thermal imaging (owing to its advantage as a noninvasive and noncontact method), in order to automatically detect the thermal discomfort level without any explicit input from the user. This research makes three contributions. First, a novel dataset of thermal recordings of 50 subjects is collected. Second, we extract and analyze features from two different thermal cameras in order to accurately detect the thermal discomfort levels of subjects. Third, we explore the capabilities of the cameras features in detecting seven levels of comfort/discomfort levels within the three categories of comfortable, cold, and hot. Our approach is expected to enable innovative adaptive control scenarios for enclosed environments as well as an important reduction in energy consumption in both buildings and vehicles.

*Address all correspondence to this author.

INTRODUCTION

Detecting thermal discomfort has been gaining a lot of interest recently in order to design energy-efficient buildings and fuel-efficient vehicles as well as provide individuals with a comfortable thermal sensation, which in return has positive consequences on climate and the environment. Existing methodologies rely on the user's manual adjustment of the suitable temperatures assumed to maintain their comfort sensation, which can result in increased energy consumption and does not ensure a permanent thermal comfort sensation.

In the U.S., the building sector consumes above 41% of the primary energy consumption, distributed as 54% energy consumption by residential buildings and 46% by commercial buildings [1]. Restoring the thermal sensation of individuals is the main factor contributing to this massive energy consumption, which is expected to increase in the next decade with global warming and carbon dioxide emissions [2, 3].

For vehicles, according to the In-Car Study run by Arbitron, drivers spend more than 2.5 hours in their vehicles daily, resulting in approximately 20 hours per week [4]. Studies showed that the air conditioning inside vehicles consumes up to 30% of the fuel in conventional internal combustion engine vehicles and can reduce the range of the vehicle's battery by up to 40% in electric

cars [5]. Other reports recommended raising the vehicle's temperature by four degrees Celsius in order to save approximately 22% of the compressor power, which also leads to a 13% increase in the coefficient of performance [6].

There exists multiple factors that affect the thermal comfort sensation of human such as subjective assessment and psychological aspects [7,8] among other different personal and environmental factors, which adds to the complexity of the detection process. However, collecting physiological signals from subjects requires contact-based devices, which is not feasible to install in buildings and vehicles for adaptive climate control systems. Hence the need arises to develop non-contact real-time approaches that automatically sense the state of thermal discomfort of the occupants and adaptively restore the thermal comfort sensation of the subjects while reducing energy and fuel consumption. Additionally, comfort level sensing is expected to result in reduced fuel consumption especially for electrical cars, which can result in additional savings and better compliance with the U.S. Corporate Average Fuel Economy (CAFE) standards.

Thermal discomfort is defined as "That condition of mind which expresses satisfaction with the thermal environment" [9]. It can also be defined as the minimum rate of nervous signals from the thermal receptors in the skin [10]. Factors affecting the thermal sensation of subjects can be divided into different personal and environmental factors. Environmental factors include air temperature, mean radiant temperature, air velocity, and relative humidity while personal factors include the metabolic rate and clothing insulation. Recently, it was shown that there was a significant difference between human thermal sensation in buildings and in vehicles [11, 12]. In particular, other factors contributed to thermal discomfort in vehicles such as the effect of solar radiation and poor interior insulation.

Previous research focused on detecting thermal discomfort in building environments to reduce energy consumption. More recently researchers started exploring the detection of thermal discomfort in vehicles to reduce fuel consumption and provide healthy and safer driving conditions. We start by surveying the approaches introduced to detect thermal discomfort in buildings.

Thermal imaging was recently used to detect thermal discomfort of human owing to its advantage as a non-contact non-invasive method. Fast Fourier transform was used to analyze thermal regions of interest from the subjects' faces in order to detect thermal discomfort [13], based on a human infrared thermography study [14]. A different study explored the relation between airflow temperatures and airflow fluctuations and human thermal sensation [15]. Infrared imaging in a mild cool office environment was used to analyze the critical indicators of thermal sensation [16]. Two control algorithms were introduced to achieve thermal comfort optimization and to achieve energy consumption minimization while maintaining the indoor thermal comfort using only-one-actuator system [17]. Haldi and Robinson [18] applied probabilistic modeling using logistic regression to study the actions of occupants sensing thermal discomfort in an indoor environment. Increased rates of thermal discomfort in buildings were reported by surveying 30,000 subjects in [19]. Fang et al. [20] analyzed the effect of air temperature, humidity, and ventilation on the thermal comfort of office workers. Another study analyzed the relation between air quality and ventilation and thermal discomfort in buildings [21]. An adaptive control model was used to detect thermal discomfort of subjects in naturally ventilated buildings [22]. In order to design energy-efficient buildings, Bessoudo [23] explored the effect of lazing type and shading properties on thermal discomfort in offices. A fuzzy model was introduced using the PMV/PPD model to effectively control thermal discomfort [24]. The relation between the size of the cooling equipment and thermal discomfort was analyzed in [25]. Humidity and air speed were reported to have increased effect on comfort sensation considering multiple factors such as air temperature, air speed, relative humidity, illumination, and metabolism of subjects using a multi-station [26].

In hot weather, vasodilation occurs, which results in increasing the width of the blood vessels. On the other hand vasoconstriction occurs in cold weather resulting in narrowing the blood vessels in the body to decrease the blood flow and keep the heat. Hoppe [27] showed that adapting thermally to hot weather was faster than cold weather. The potential of using wearable sensors in detecting thermal discomfort in buildings was discussed in [28]. A study detected a correlation between the forehead temperature and the subjects' thermal sensation by collecting data from 10 subjects [29]. ThermalSense is another approach that utilized thermographic imaging to look for the physiological markers of vasodilation or vasoconstriction in order to detect thermal comfort [30].

More recently, sensing thermal discomfort in vehicles gained more interest. In particular, an analysis was conducted to analyze the personal and environmental factors that affect the discomfort sensation in vehicles [11]. Studies showed that the discomfort sensation in vehicles differs from buildings as it includes other factors such as the effect of solar radiation, poor interior insulation, and the non-uniformity of the average radiant temperature [12]. Vehicles thermal discomfort parameters were explored to improve the detection methods and it was reported that the relative air humidity and the inside temperature were the main contributors to thermal discomfort in vehicles [31].

Multimodal sensing had been recently used to detect thermal discomfort. Dang et al. [32] developed a navigation system that chooses passes to reduce thermal discomfort for pedestrians. A preliminary study showed the potential of combining thermal imaging with certain body signals in improving thermal discomfort detection rates [33, 34].

Hence, in this paper we propose a non-contact approach to detect thermal discomfort levels of subjects in indoor environments similar to that in buildings and vehicles using thermal imaging. Thermal imaging is a non-invasive non-contact mean

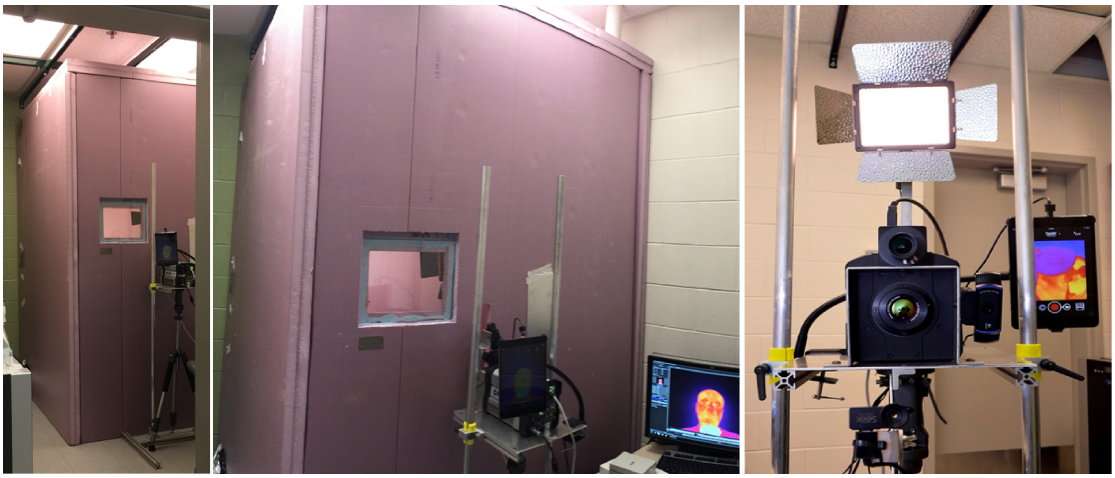

FIGURE 1. The experimental station including an insulating enclosure and thermal cameras.

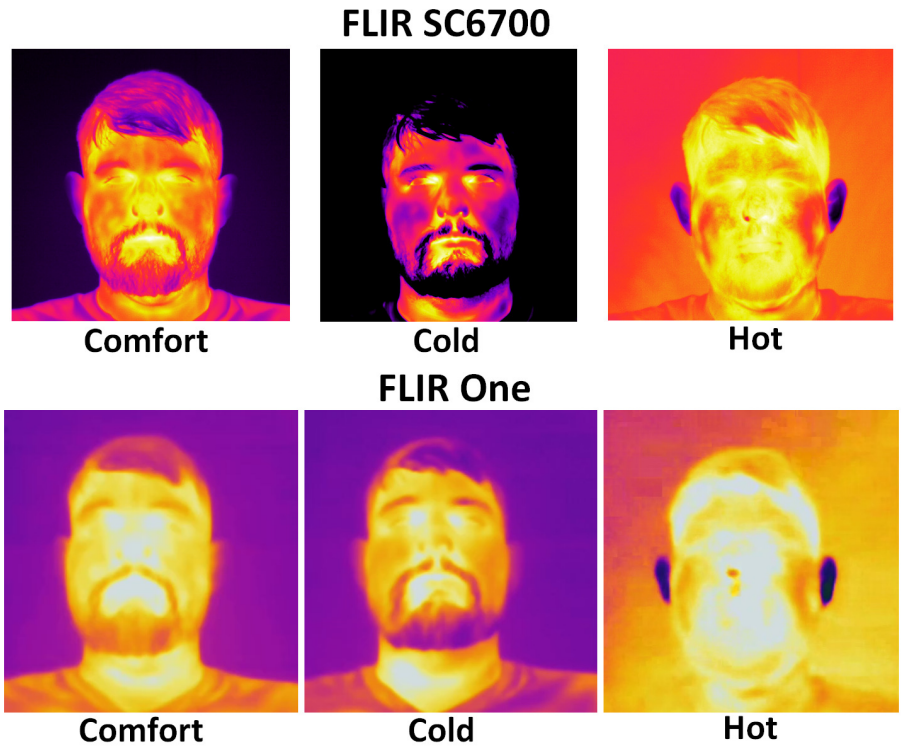

FIGURE 2. Examples of the recorded frames from FLIR SC6700 (top row), and FLIR One (bottom row). The images represent a comfort state (left), a cold discomfort state (middle), and a hot discomfort state (right).

to capture thermal measurements from heat-emitting sources, which has multiple application in different fields such as the medical and military fields [35–37].

In particular, this paper makes three contributions. First, a novel dataset of thermal recordings of 50 subjects is collected. Three scenarios are conducted, where the subjects are placed in comfortable conditions, in a cold environment, and in a hot environment using an insulating enclosure. The desired environmental conditions inside the enclosure are maintained using a heat pump. Second, we extract and analyze features from two different thermal cameras in order to accurately detect the thermal discomfort levels of subjects. The cameras include a state-of-

the-art scientific grade FLIR camera and a cost effective thermal camera. Thus, the feasibility of using an inexpensive thermal camera is investigated, especially for usage in vehicles and in different rooms in cost-effective homes. On the other hand, the scientific grade FLIR camera can be installed in smart homes and business buildings. Third, we explore the capabilities of the cameras features in detecting seven different comfort/discomfort levels within the three categories of comfortable, cold, and hot.

DATASET COLLECTION

Devices

Two different thermal cameras were used to accurately detect the thermal discomfort levels of subjects. The cameras include a state-of-the-art scientific grade FLIR camera and a cost effective thermal camera. We used a FLIR SC6700 thermal camera with a resolution of 640x512 and 7.2 M electrons capacity, reaching a frame rate of approximately 100 frames per second. We set it at 60 frames per second for our experiments. A low-cost FLIR One thermal camera was also used to capture thermal recordings of the subjects during different thermal comfort and discomfort stages.[1] The reason behind choosing this low-end camera is the feasibility of installing such cameras that fall under $250 in vehicles without any significant changes in the vehicle price. However, the state-of-the-art FLIR SC6700 thermal camera can be installed in different buildings and homes. The FLIR One camera was connected to an IPad to save the recorded videos using the FLIR One app.

Subjects

Experiments were conducted inside a lab at the University of Michigan. The lab features an insulating enclosure (W x L x H is 2m x 2m x 2.5m) with a seat for the subjects and two thermal cameras trained at the face of the human subjects. Our dataset consists of recordings collected from 50 human subjects. The subjects included 32 males and 18 females of different ethnic backgrounds, with an age range between 18 and 60.

Experimental Procedure

In order to simulate a small enclosed environment similar to that found in a vehicle or a room, we built an enclosure with insulating material for complete isolation from the room temperature. The enclosure was connected to a heat pump in order to blow hot and cold air. The relative humidity was in the 40-60% range. The enclosure contained a seat for the subjects to sit comfortably as well as a fan and a heater to increase the subjects' sensation of cold and hot, respectively. The enclosure also had a slit to capture videos using the thermal cameras. A picture of this system can be seen in Figure 1. The subjects were asked to sit comfortably in the seat in the enclosure. The data collection process included three stages.

Comfort. The subjects were asked to stay in the building where the experiments were conducted for a period of time, to adapt to the indoor temperature and feel thermally comfortable. After spending some time in the building, they were asked to sit in the enclosure and stay inside to the end of the experiments. After the subjects confirmed they were feeling thermally comfortable, they were recorded for four minutes in this state. The enclosure temperature in this stage ranged between approximately 20^oC to 24^oC.

Cold Discomfort. As the subjects were sitting inside the enclosure, cold air was blown inside using the heat pump and the fan. This process continued for approximately 20 minutes until the enclosure temperature reached approximately 16^oC (61^oF). The subjects were then recorded for four minutes with the cold air continuously blowing.

Hot Discomfort. In this stage, hot air was blown into the enclosure using both the heat pump and a 2000W electric heater (to decrease the time it takes for the air inside the enclosure to reach the target temperature) while the subjects were sitting inside. This process continued for approximately 10 minutes until the enclosure temperature exceeded 35^oC (95^oF). The subjects were again recorded for four minutes with continuous blow of hot air.

Thermal Sensation Rating To further evaluate the comfort/discomfort level of the subjects, the Predicted Mean Vote/Predicted Percentage of Dissatisfied or PMV/PPD model developed by Fanger [38] was used, which assumed steady state conditions in an indoor environment. The model is the most famous thermal discomfort model and can be used in air-conditioned buildings, which resembles our setup. The PMV rates the thermal sensation of the subjects on a scale of (-3) for cold to (3) for hot. The surveyed individuals choose a value on the thermal scale to express their thermal sensation.

At each of the three stages, the subjects were asked to rate their thermal sensation using the PMV scale. All the subjects rated the comfort stage as "0", which represented the thermally neutral state on the PMV scale. For cold discomfort, the subjects' ratings ranged from -1 to -3. Similarly for the hot stage, their ratings ranged from 1 to 3.

It should be noted that the thermal recordings using the FLIR SC6700 camera were collected from all of the 50 subjects. However, due to an error in the FLIR One software update, thermal recordings from the FLIR One camera were saved from only 22 subjects.

[1] http://www.flir.com/flirone/content/?id=81730

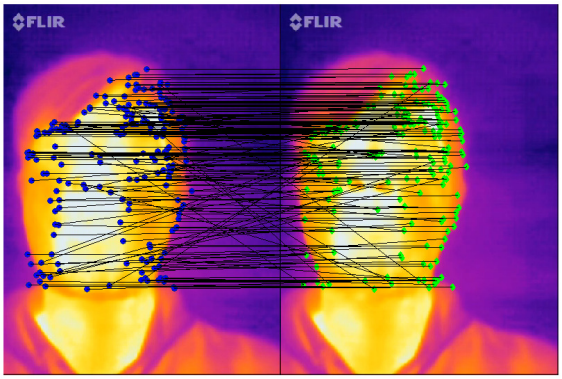

FIGURE 3. Detecting and tracking interesting points between frames from the FLIR One camera, which are usually found at sharper changes in colors, i.e., changes in temperatures.

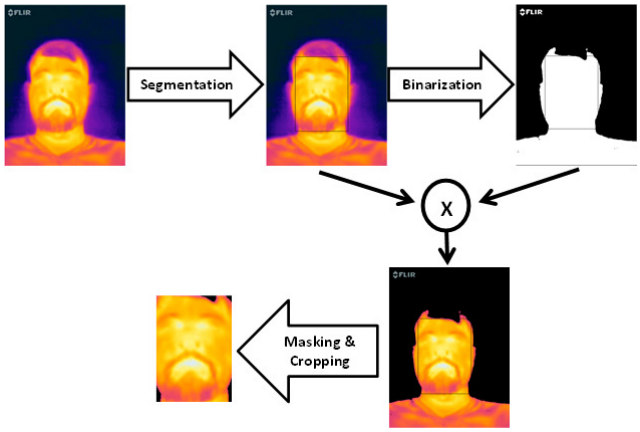

FIGURE 4. The process of segmenting, binarizing, masking, and cropping the thermal faces.

NON-CONTACT APPROACH

To represent the thermal signatures extracted from the subjects' faces, three steps were performed, namely, face segmentation, face tracking, and thermal map formation. The same steps were followed for the recordings of both thermal cameras.

Examples of the frames recorded from both cameras are shown in Figure 2. The images on the top are from the FLIR SC6700 camera while the bottom images are from FLIR One. The states presented are comfortable (left), cold discomfort (middle), and hot discomfort (right). It can be noticed that in both cases darker colors presenting lower temperatures are associated with the cold state and lighter colors presenting higher temperatures are associated with hotter states. As depicted in the figure, these trends as well as the resolution are significantly better with the FLIR SC6700 frames. As expected, the temperature distributions in different areas of the faces are much clearer in the state-of-the-art camera, which can be explored in future work to determine which regions in the face are most capable if indicating the thermal sensation of the subjects.

Tracking Thermal Faces

First, the thermal faces of the subjects were manually segmented from the first frame of each of the video recordings. Automatic methods of face detection did not perform well on thermal images especially with the low resolution of FLIR One camera. We will leave the development of an automatic detection of thermal faces for future work. Once the faces were segmented, interesting points were located in the bounding boxes of the detected faces. The points were detected based on the Shi-Tomasi corner detection algorithm [39] by computing the weighted sum of square difference between two successive frames. We used the Iron color palette for the FLIR One camera, where lighter colors mapped higher temperatures and darker colors mapped lower temperatures. For the FLIR SC6700, the raw thermal recordings were used. Hence, the interesting points were usually located where sharper changes in the colors existed as seen in Figure 3, which potentially indicated the existence of a blood vein that controls, to a large extent, the temperature of the surrounding region.

Once the interesting points were detected, they were tracked using a fast Kanade-Lucas-Tomasi (KLT) tracking algorithm [40, 41] as can be seen in Figure 3. KLT is a famous tracking method known for accurate tracking of objects that have visual texture without change in shape over time. The algorithm assumes a small displacement between the pixels in two successive frames, which suited our tracking requirements. The subjects were not forced to avoid head movements, but they did not make any extreme movements. To increase the accuracy of the tracking approach, the Forward-Backward Error [42] was calculated by tracking the points back and forth between frames in order to eliminate outliers and avoid the uncertainty with some points. The face bounding box was then reconstructed using geometric transformation [43], which globally estimated the interesting points transformation based on similarity. Once the points were mapped, the new boundary box was geometrically determined.

Stage-wise Experiments
Thermal Map

In order to extract thermal features from the tracked faces, masking, binarization, and cropping of the facial regions were used. In particular, the frames of the tracked faces were binarized to form a holistic shape of the faces and eliminate the background. For FLIR One, this was conducted under the assumption that the backgrounds of the faces were not heat emitting sources (darker colors) and hence, would be transformed into black pixels. For FLIR SC6700, we set a temperature of 26.94^{o}C (80.5^{o}F) as a threshold below which any temperature is set to zero as to eliminate the background behind the subjects. The binarized im-

TABLE 1. Overall accuracy as well as the recall of each of the comfort, cold discomfort, and hot discomfort classes for FLIR SC6700 using the statistical features in addition to the histogram of 20, 60, 120, 180 and 255 bins from all 50 subjects.

FLIR SC6700	Baseline	Hist20	Hist60	Hist120	Hist180	Hist255
Accuracy	33.3	**99.3**	98.0	98.0	98.0	98.0
Comfort	33.3	**98.0**	96.0	96.0	96.0	96.0
Cold	33.3	**100.0**	98.0	98.0	98.0	98.0
Hot	33.3	**100.0**	**100.0**	**100.0**	**100.0**	**100.0**

age and the original face were then multiplied to restore the actual face. Finally the face region was cropped and a thermal map was constructed as seen in Figure 4.

For FLIR One, the thermal map was created from the Hue Saturation Value (HSV) pixel representation by extracting the average of the pixels values of the face, the maximum pixel value presenting the highest temperature in the face, the minimum pixel value presenting the lowest temperature of the face, the standard deviation, which measured the difference between the minimum and maximum temperatures, the mean of the 10% highest pixel values, and a histogram of 60, 120, 180, and 255 bins over the values of the pixels in the face to form a total of 195, 375, 555, and 780 thermal features for all the three HSV channels.

For FLIR SC6700, statistical measurements and histograms were computed directly from the raw temperatures in the cropped faces. In particular, the maximum, minimum, mean, mean of the 10% highest values, and standard deviation of the temperatures were calculated as well as a temperature histogram of 20, 60, 120, 180, and 255 bins.

The histogram was normalized to form a probability distribution over all bins. The thermal features from all the frames were averaged to create a single thermal feature vector per video response for each of the thermal cameras.

EXPERIMENTAL SETUP FOR DETECTING DISCOMFORT

We perform two sets of experiments using machine learning. Training instances (feature vectors) are used to train the classifier to learn the differences between different discomfort stages, and then the classifier is used to predict the label on a new (unseen) instance. First, we conduct stage-wise experiments where the unseen recordings are classified into either comfortable, cold, or hot. Second, we conduct a PMV-based classification where we extended our classification process in order to classify unseen instances into one comfort level, three cold discomfort levels, and three hot discomfort levels

A decision tree classifier was trained using the thermal feature vectors from both cameras separately in order to classify unseen instances as comfort, cold, or hot. It should be noted that for FLIR SC6700, all feature vectors from the 50 subjects were used, while for the FLIR One, feature vectors from only 22 subjects were used. In order to provide a fair comparison, we also experiment the feature vectors from the same set of 22 subjects from the FLIR SC6700 camera.

We use Leave-one-subject-out cross validation scheme. This scheme indicates that all the recordings of all the subjects are used to train the classifier except for the three recordings of one subject, which are held out for testing. This process repeats until all the recordings of all subjects are used once for testing. For example, this process repeats 50 times for 50 subjects, testing three instances of one of the subjects at each fold. We report the average classification accuracy as well as the recall of each class. Accuracy refers to the ratio of correctly classified instances to the total number of tested instances. Recall refers to the ratio of correctly classified instances of a specific class (comfort, cold, or hot) to the number of instances belonging only to this class. The results are also compared to the baseline performance, which is based on random guessing.

EXPERIMENTAL RESULTS

Stage-wise Experiments

Table 1 lists the overall accuracy and the recall of the comfort, cold discomfort, and hot discomfort classes as well as the baseline performance, for FLIR SC6700 using the statistical features in addition to the histogram of 20, 60, 120, 180 and 255 bins from all 50 subjects. The table indicates a superior performance using different sizes of bins reaching at least 98% in the overall accuracy. The different histogram sizes exhibit similar performance except for the 20 bins, which exceeds 99% accuracy. This indicates that the scientific thermal camera is capable of sensing the thermal sensation of different subjects with great confidence.

Table 2 lists the overall accuracy and the recall of the comfort, cold discomfort, and hot discomfort classes as well as the baseline performance, for both the FLIR SC6700 and FLIR One cameras using the statistical features in addition to the histogram of 60, 120, 180 and 255 bins from 22 subjects. In order to provide a fair comparison, we repeated the experiments for the FLIR SC6700 using the recordings of the same set of 22 subjects saved by FLIR One.

Four observations can be noticed from the table. First, the performance of the instances used from FLIR SC6700 drops slightly as the number of subjects drops to 22, and hence the

TABLE 2. Overall accuracy as well as the recall of each of the comfort, cold discomfort, and hot discomfort classes for FLIR SC6700 and FLIR One cameras using the statistical features in addition to the histogram of 60, 120, 180 and 255 bins from the 22 subjects.

		FLIR SC6700				**FLIR One**			
	Baseline	Hist60	Hist120	Hist180	Hist255	Hist60	Hist120	Hist180	Hist255
Accuracy	33.3	97.0	97.0	97.0	97.0	77.3	68.2	75.8	74.2
Comfort	33.3	95.5	95.5	95.5	95.5	59.1	54.5	77.3	77.3
Cold	33.3	95.5	95.5	95.5	95.5	77.3	63.6	72.7	68.2
Hot	33.3	100.0	100.0	100.0	100.0	95.5	86.4	77.3	77.3

TABLE 3. Overall accuracy as well as the recall of each of the comfort, three cold discomfort, and three hot discomfort classes for FLIR SC6700 using the statistical features in addition to the histogram of 20, 60, 120, 180 and 255 bins from all 50 subjects.

FLIR SC6700	No.	Baseline	Hist20	Hist60	Hist120	Hist180	Hist255
Accuracy		33.3	**63.9**	55.8	51.7	52.4	56.5
Comfort	22	33.3	**100.0**	95.9	95.9	93.9	91.8
Cold -1	6	9.1	**64.7**	23.5	41.2	41.2	0
Cold -2	9	13.6	**45.0**	25.0	20.0	20.0	**45.0**
Cold -3	7	10.6	33.3	33.3	33.3	16.7	**50.0**
Hot 1	7	10.6	21.4	21.4	0	28.6	**50.0**
Hot 2	11	16.7	62.1	**65.5**	48.3	48.3	55.2
Hot 3	4	6.1	0	0	0	0	0

classifier is trained with lower number of instances. Second, the performance using the scientific thermal camera is clearly better than that using FLIR One. Third, the performance using FLIR One, however, is significantly better than the baseline exceeding 77% accuracy. Fourth, it can be noted that the "Hot" class achieves the highest recall among all classes using both cameras, which indicates that it is easier to detect.

PMV-based Experiments

Table 3 lists the overall accuracy and the recall of the comfort, Cold -1, Cold -2, and Cold -3, Hot 1, Hot 2, and Hot 3 classes as well as the baseline performance, for FLIR SC6700 using the statistical features in addition to the histogram of 20, 60, 120, 180 and 255 bins from all 50 subjects. Cold -1 to -3 and Hot 1 to 3 reflect the ratings determined by the subjects using the PMV scale, as mentioned earlier, ranging between -3 representing the coldest level to 3 representing the hottest level. The second column in the table represents the number of instances for each class. The table indicates that instances from the scientific camera is capable of detecting different thermal discomfort classes exceeding 60% overall accuracy. In particular, the histograms of 20 bins followed by 255 bins achieve the best performance. The performance exceeds that of the baseline in the majority of the cases. However, it can be noted that as the distribution of the instances among the classes results in lower number of training instances for the classifier per class, the performance drops compared to classifying unseen instances as only comfortable, cold, and hot. For example, the Hot 3 class only has four instances which is not sufficient for the classifier to learn to predict this class, resulting in complete failure in detecting the Hot 3 state.

Table 4 lists the overall accuracy and the recall of each of the comfort, three cold discomfort, and three hot discomfort classes as well as the baseline performance, for both the FLIR SC6700 and FLIR One cameras using the statistical features in addition to the histogram of 60, 120, 180 and 255 bins from 22 subjects.

As in the earlier cases, the performance using instances from FLIR SC6700 is better compared to that of FLIR One. However, the margin of improvement is not as significant as it was earlier in detecting comfort, cold, and hot. This indicates that the low-cost FLIR One camera is still capable of providing acceptable performance. In fact, the instances from FLIR One achieve higher recall for the Hot 1 and Hot 2 classes. Moreover, the

TABLE 4. Overall accuracy as well as the recall of each of the comfort, three cold discomfort, and three hot discomfort classes for FLIR SC6700 and FLIR One cameras using the statistical features in addition to the histogram of 60, 120, 180 and 255 bins from the 22 subjects.

			FLIR SC6700				FLIR One			
	No.	Baseline	Hist60	Hist120	Hist180	Hist255	Hist60	Hist120	Hist180	Hist255
Accuracy		33.3	53.0	45.5	48.5	47.0	42.4	40.9	45.5	45.5
Comfort	22	33.3	90.9	90.9	90.9	90.9	54.5	54.5	68.2	63.6
Cold -1	6	9.1	50.0	0	16.7	16.7	16.7	0	0	16.7
Cold -2	9	13.6	33.3	33.3	55.6	77.8	22.2	22.2	33.3	33.3
Cold -3	7	10.6	28.6	57.1	57.1	14.3	14.3	14.3	0	0
Hot 1	7	10.6	28.6	0	14.3	0	85.7	85.7	85.7	85.7
Hot 2	11	16.7	45.5	27.3	9.1	18.2	54.5	54.5	54.5	54.5
Hot 3	4	6.1	0	0	0	0	0	0	0	0

performance exceeds the baseline in the majority of cases. By cross-referencing Table 3, it can once again be concluded that having more instance to train the classifier results in improved performance using FLIR SC6700.

In order to understand the reason behind the improved performance using the scientific thermal camera, we visualize the average temperatures detected in the faces of the 22 subjects as can be seen in Figure 5. The figure shows the mean average face temperatures sorted by the comfort state values for FLIR SC6700 (left). The figure also shows the scaled mean face temperatures for FLIR One camera, calculated from the average pixel values of the faces scaled by a temperature measurement in the middle of the faces provided by the FLIR One software.

The figure shows that the curves of the comfortable, cold, and hot states are well separated using the scientific thermal camera. On the other hand, the comfortable and cold curves as well as the hot and comfortable curves intersect for multiple subjects using FLIR One, indicating that this camera is less capable of providing the separation required between different discomfort states in order to achieve the optimal performance of detecting the thermal sensation of the subjects.

Furthermore, the human body needs a relatively longer time to go from the comfort stage to the cold discomfort state and needs approximately half that time to transfer from the cold discomfort state to the hot discomfort state. This also indicates that the human body has faster adaptation to a hot environment.

CONCLUSION

Thermal discomfort detection can have positive consequences on climate and the environment, and results in designing energy-efficient buildings and fuel-efficient vehicles as well as provides individuals with a comfortable thermal sensation. As people move freely in buildings and cannot have contact-based devices while driving, we introduced a non-contact, non-invasive approach that relies on the thermal features obtained from thermal imaging, in order to automatically detect the thermal discomfort states without any explicit input from the user. This can eventually result in developing adaptive thermal comfort models that can predict the level of discomfort of the building's or vehicle's occupants and restore their thermal comfort.

In particular, we introduced a novel dataset of thermal recordings of 50 subjects, with three scenarios, where the subjects are placed in comfortable conditions, in a cold environment, and in a hot environment using an insulating enclosure. Moreover, we extracted and analyzed features from two different thermal cameras in order to accurately detect the thermal discomfort levels of subjects using a scientific grade FLIR camera and a cost effective thermal camera. Furthermore, we explored and compared the capabilities of the cameras features in detecting differ-

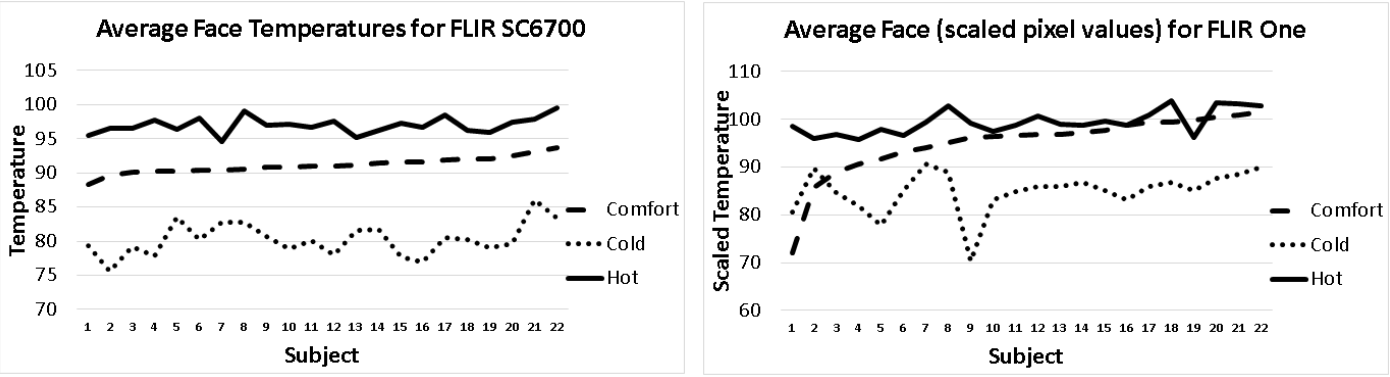

FIGURE 5. Sorted mean face temperatures and sorted scaled face temperatures (pixel values) of the 22 subjects through the comfort, cold discomfort, and hot discomfort stages for FLIR SC6700 (left) and FLIR One (right).

ent discomfort levels within the three categories of comfortable, cold, and hot using stage-wise and PMV-based experiments.

The results showed that the scientific thermal camera had higher capability of indicating thermal discomfort of the subjects with great confidence. However, the low-cost thermal camera also exceeded 70% accuracy and outperformed the baseline, which indicates it can be used in vehicles and in different rooms in apartments/houses. As the classification system was extended to detect the comfortable class, three cold states, and three hot states using the PMV model, the performance dropped indicating the need of more training instances for the seven different classes. Moreover, the margin of improvement using the scientific camera over FLIR One is reduced in case of predicting seven comfort/discomfort states. In general, our research indicates the feasibility of installing non-contact thermal imaging systems in homes ,personal assistant robots, and in vehicles to detect thermal discomfort, and eventually designing adaptive systems that save energy and fuel.

It was also observed that it took almost double the time to reaching a certain level of cold discomfort compared to hot discomfort. This could be explained using thermoregulation as well as the first law of Thermodynamics. When the human body is being cooled, the energy that needs to be expelled from the body is higher due to the metabolic heat production. When the body is heated, the metabolic heat does not need to be expelled. This can indicate that humans adapt thermally to heat faster than cold.

Our tracking approach of the thermal faces would be very convenient for thermal discomfort detection in vehicles due to the incapability of the driver to make extreme movements and given that our approach assumes small displacement between successive frames. However, as there is more space for the subjects to move in different rooms in buildings, a larger tracking framework will be required for accurate thermal discomfort detection. Alternatively, a synchronized version of our tracking approach can be developed if multiple low-cost thermal cameras are installed in the same room.

ACKNOWLEDGMENT

REFERENCES

[1] Administration, U. E. I., 2013. Residential energy consumption survey. Tech. rep., May.

[2] Mller, N., Kuttler, W., and Barlag, A.-B., 2014. "Counteracting urban climate change: adaptation measures and their effect on thermal comfort". *Theoretical and Applied Climatology,* ***115***(1-2), pp. 243–257.

[3] Aebischer, B., Catenazzi, G., and Jakob, M., 2007. "Impact of climate change on thermal comfort, heating and cooling energy demand in europe". In Proceedings ECEEE 2007 Summer Study "Saving Energy Just Do It!", pp. 23–26.

[4] Williams, D., 2009. The arbitron national in-car study. Tech. rep., Arbitron Inc.

[5] Farrington, R., and Rugh, J., 2000. *Impact of Vehicle Air-Conditioning on Fuel Economy, Tailpipe Emissions, and Electric Vehicle Range: Preprint*. National Renewable Energy Laboratory, Sep.

[6] Subiantoro, A., Ooi, K. T., and Stimming, U., 2014. "Energy saving measures for automotive air conditioning (ac) system in the tropics". *International refrigeration and air conditioning conference*.

[7] Hoppe, P. R., and Seidl, H. A., 1991. "Problems in the assessment of the bioclimate for vacationists at the seaside". *International Journal of Biometeorology,* ***35***(2), pp. 107–110.

[8] Rohles, F. H., 2007. "Temperature and temperament: A psychologist looks at comfort". *ASHRAE Transactions,* ***49***, pp. 14–19.

[9] , 1997. "Ashrae (american society of heating and refrigerating engineers)". In Handbook of Fundamentals: Physio-

logical Principles, Comfort, Health.
[10] Mayer, E., 1993. "Objective criteria for thermal comfort". *Building and Environment,* ***28***(4), pp. 399 – 403.
[11] Simion, M., Socaciu, L., and Unguresan, P., 2016. "Factors which influence the thermal comfort inside of vehicles". *Energy Procedia,* ***85***, pp. 472 – 480.
[12] Danca, P., Vartires, A., and Dogeanu, A., 2016. "An overview of current methods for thermal comfort assessment in vehicle cabin". *Energy Procedia,* ***85***, pp. 162 – 169. EENVIRO-YRC 2015 - Bucharest.
[13] Fabrice De Oliveira, Sophie Moreau, C. G., and Dittmar, A., 2007. "Infrared imaging analysis for thermal comfort assessment". In 29th Annual International Conference of the IEEE Engineering in Medicine and Biology Society, pp. 3373–3376.
[14] Gulyaev, Y. V., Markov, A. G., Koreneva, L. G., and Zakharov, P. V., 1995. "Dynamical infrared thermography in humans". *IEEE Engineering in Medicine and Biology Magazine,* ***14***(6), pp. 766–771.
[15] Oliveira, F. D., and Moreau, S., 2009. "Assessment of thermal environment sensation for various climatic conditions and fluctuating air flow". In EACWE 5.
[16] Zeiler, W., Boxem, G., van Houten, R., Vissers, D., and Maaijen, R., 2012. "The human leading the thermal comfort control". In Twelfth International Conference for Enhanced Building Operations, pp. 23–26.
[17] Freire, R. Z., Oliveira, G. H., and Mendes, N., 2008. "Predictive controllers for thermal comfort optimization and energy savings". *Energy and Buildings,* ***40***(7), pp. 1353 – 1365.
[18] Haldi, F., and Robinson, D., 2008. "On the behaviour and adaptation of office occupants". *Building and Environment,* ***43***(12), pp. 2163 – 2177.
[19] Huizenga, C., Abbaszadeh, S., Zagreus, L., and Arens, E. A., 2006. "Air quality and thermal comfort in office buildings: Results of a large indoor environmental quality survey". In Healthy Buildings, pp. 393–397.
[20] Fang, L., Wyon, D. P., Clausen, G., and Fanger, P. O., 2004. "Impact of indoor air temperature and humidity in an office on perceived air quality, sbs symptoms and performance". *Indoor Air,* ***14***, pp. 74–81.
[21] Zheng, G., Jing, Y., Huang, H., and Ma, P., 2009. "Thermal comfort and indoor air quality of task ambient air conditioning in modern office buildings". In Information Management, Innovation Management and Industrial Engineering, 2009 International Conference on, Vol. 2, pp. 533–536.
[22] Ye, X. J., Zhou, Z. P., Lian, Z. W., Liu, H. M., Li, C. Z., and Liu, Y. M., 2006. "Field study of a thermal environment and adaptive model in shanghai". *Indoor Air,* ***16***(4).
[23] Bessoudo, M., 2008. *Building Façades and Thermal Comfort: The Impacts of Climate, Solar Shading, and Glazing on the Indoor Thermal Environment*. VDM Publishing.
[24] Homod, R. Z., Sahari, K. S. M., Almurib, H. A., and Nagi, F. H., 2012. "{RLF} and {TS} fuzzy model identification of indoor thermal comfort based on pmv/ppd". *Building and Environment,* ***49***(0), pp. 141 – 153.
[25] Hamdy, M., Hasan, A., and Siren, K., 2011. "Impact of adaptive thermal comfort criteria on building energy use and cooling equipment size using a multi-objective optimization scheme". *Energy and Buildings,* ***43***(9).
[26] Ismail, A. R., Jusoh, N., Ibrahim, M. H., Panior, K. N., Zin2, M. Z. M., Hussain, M. A., and Makhtar3, N. K., 2010. "Thermal comfort assessment in computer lab: A case study at ungku omar polytechnic malaysia". In National Conference in Mechanical Engineering Research and Postgraduate Students, pp. 408–416.
[27] Hoppe, P., 2002. "Different aspects of assessing indoor and outdoor thermal comfort". *Energy and Buildings,* ***34***(4).
[28] Abdallah, M., Clevenger, C., Vu, T., and Nguyen, A., 2016. "Sensing occupant comfort using wearable technologies". In Construction Research Congress 2016, pp. 940–950.
[29] Pavlin, B., Pernigotto, G., Cappelletti, F., Bison, P., Vidoni, R., and Gasparella, A., 2017. "Real-time monitoring of occupants thermal comfort through infrared imaging: A preliminary study". *Buildings,* ***7***(10).
[30] Ranjan, J., and Scott, J., 2016. "Thermalsense: Determining dynamic thermal comfort preferences using thermographic imaging". In Proceedings of UbiComp 2016, ACM.
[31] Musat, R., and Helerea, E., 2009. "Parameters and models of the vehicle thermal comfort". In Electrical and Mechanical Engineering 1, Acta Universitatis Sapientiae, pp. 215–226.
[32] Dang, C., Iwai, M., Tobe, Y., Umeda, K., and Sezaki, K., 2013. "A framework for pedestrian comfort navigation using multi-modal environmental sensors". *Pervasive and Mobile Computing,* ***9***(3), pp. 421 – 436.
[33] Burzo, M., Abouelenien, M., Pérez-Rosas, V., Wicaksono, C., Tao, Y., and Mihalcea, R., 2014. "Using infrared thermography and biosensors to detect thermal discomfort in a buildings inhabitants". In ASME International Mechanical Engineering Congress and Exposition, American Society of Mechanical Engineers, pp. 1–11.
[34] Burzo, M., Wicaksono, C., Abouelenien, M., erez Rosas, V. P., Mihalcea, R., and Tao, Y., 2014. "Multimodal sensing of thermal discomfort for adaptive energy saving in buildings". In iiSBE Net Zero Built Environment 2014 Symposium.
[35] Arora, N., Martins, D., Ruggerio, D., Tousimis, E., Swistel, A. J., Osborne, M. P., and Simmons, R. M., 2008. "Effectiveness of a noninvasive digital infrared thermal imaging system in the detection of breast cancer". *The American Journal of Surgery,* ***196***(4), pp. 523 – 526.
[36] Ng, E.-K., 2009. "A review of thermography as promising

non-invasive detection modality for breast tumor". *International Journal of Thermal Sciences,* ***48***(5), pp. 849 – 859.

[37] Garbey, M., Sun, N., Merla, A., and Pavlidis, I., 2007. "Contact-free measurement of cardiac pulse based on the analysis of thermal imagery". *IEEE Transactions on Biomedical Engineering,* ***54***(8), pp. 1418–1426.

[38] Ashrae, 2007. "Ashrae publishes residential air quality standard".

[39] Shi, J., and Tomasi, C., 1994. "Good features to track". In IEEE Computer Society Conference on Computer Vision and Pattern Recognition, CVPR, pp. 593–600.

[40] Sinha, S. N., Frahm, J.-m., Pollefeys, M., and Genc, Y., 2006. Gpu-based video feature tracking and matching. Tech. rep., The University of North Carolina at Chapel Hill.

[41] Tomasi, C., and Kanade, T., 1991. Detection and tracking of point features. Tech. rep., Carnegie Mellon University, April.

[42] Kalal, Z., Mikolajczyk, K., and Matas, J., 2010. "Forward-backward error: Automatic detection of tracking failures". In 20th International Conference on Pattern Recognition (ICPR), pp. 2756–2759.

[43] Hartley, R., and Zisserman, A., 2003. *Multiple View Geometry in Computer Vision*. Cambridge books online. Cambridge University Press.